JOURNAL OF SOLID STATE CHEMISTRY 93, 443–453 (1991)

Composition and Cation–Vacancy Distribution of Cation-Deficient Mn/Fe Spinel Oxides

J. M. JIMENEZ MATEOS, W. JONES*, J. MORALES, AND J. L. TIRADO

*Departamento de Química Inorgánica e Ingeniería Química, Facultad de Ciencias, Universidad de Córdoba, San Alberto Magno s/n, 14004 Córdoba, Spain; and *Department of Chemistry, University of Cambridge, Lensfield Road, Cambridge CB2 1EW, United Kingdom*

Received January 16, 1990; in revised form March 6, 1991

Chemical composition and vacancy ditribution are studied in cation-deficient Mn/Fe spinel oxides of general formula $Fe_{3-x}Mn_xO_{4+y}$ prepared by the thermal decomposition of mixed carbonates. An oxygen/metal ratio in the 1.5–1.6 range is found for samples obtained at 400°C in an air atmosphere. In addition, a significant content of Mn(IV) ions can be derived from chemical and XRD data. The Mössbauer data of these samples reveal the effects of small particle size as well as isolating effects of the Fe(III) ions in *B* sites by *A*-site cation vacancies. These effects increase with Mn content. For samples prepared at 600°C, the XRD data and Mössbauer data are interpreted in terms of a higher particle size and lower vacancy content than those found at 400°C. At both temperatures, the cation vacancies found in *B*-sites are ordered in a γ-Fe_2O_3-type superstructure when the Mn content is lower than 0.6.

Introduction

Manganese-iron oxides as well as Zn-substituted derivatives have been the subject of many research works due to the significance of their magnetic and electrical properties (*1–3*). In these systems, cation distribution and nonstoichiometry are highly influenced by the preparation conditions (*4, 5*). For a nearly stoichiometric spinel, X-ray diffraction data showed that all cation vacancies were located in the octahedral sites (*6*).

Particular attention has recently been paid to the oxidation behavior of fine grained Mn-ferrites previously prepared by thermal decomposition of mixed oxalates (*7–9*). In this process, Mn(III) ions in octahedral sites oxidize to Mn(IV) while Mn(II) ions in tetrahedral sites remain unaltered (*7*). A certain ordering of vacancies was detected by IR spectroscopy (*8*).

An alternative procedure to obtain highly dispersed spinel oxides with high cation oxidation states is the low temperature decomposition of mixed carbonates (*10, 11*). For mixed Co/Mn spinels (*10*), this method allows the occurrence of a high content of vacancies that are ordered in a tetragonal superstructure. Here we describe the structural characteristics of Mn/Fe cation-deficient spinels prepared from mixed carbonates on the basis of XRD, electron microscopy, and Mössbauer spectroscopy.

Experimental

Mn/Fe carbonates were prepared by mixing a 1.0 *M* solution of $NaHCO_3$ and an 0.5

0022-4596/91 $3.00

M solution of the divalent cations under a continuous CO_2 flow (*12*). Total Fe and Mn contents of the samples were determined by atomic absorption spectrometry. The homogeneity of Mn/Fe ratios was checked by electron microprobe measurements. The average oxidation state of metal ions in the samples was determined by a previously described method (*10*). Samples were dissolved in an aqueous solution of H_2SO_4 and HCl in the presence of Fe^{+2} under a continuous flow of Ar. The solution was titrated with standard $K_2Cr_2O_7$ using diphenilamine as indicator. A blank titration was carried out under the same conditions. The difference between the titrations was assigned to the total content of oxidating species (Mn(III) and Mn(IV)) and was used to calculate the O/M ratios.

Differential Scanning Calorimetry (DSC) traces were obtained with a Mettler TA 3000 apparatus. Mössbauer spectra were obtained with a constant accelerator spectrometer with a 10 mCi $^{57}Co/Rh$ source and were calibrated against α-Fe. XRD data were collected with a Siemens D500 diffractometer provided with Cu$K\alpha$ radiation and graphite monochromator. X-ray diffraction line broadening analysis was carried out by recording the profiles by the step-scan technique and applying the procedure described in Ref. (*13*). Electron micrographs were obtained with a JEOL 200 CX apparatus. N_2 adsorption data were used to obtain the specific surface area by the BET method (*14*).

Results and Discussion

Mixed carbonates of general formula $Mn_xFe_{1-x}CO_3$ ($0 \leq x \leq 1$) were obtained as monophasic solids with a high homogeneity in composition as shown by XRD and electron microprobe measurements. The ability of the preparation method to obtain mixed carbonate precursors in a wide range of compositions has been previously stated (*10–12, 15*).

The thermal behavior of the Mn/Fe carbonates was followed by the DSC traces recorded under static air and dynamic N_2 atmosphere. These curves are shown in Fig. 1 for selected compositions. The temperature for endothermal decomposition increased with Mn content, in agreement with previously reported data on the thermal decomposition of Fe and Mn carbonates (*16*). The exothermal effect following the endotherm can be associated with oxidation processes by O_2, as these effects were not found in the DSC traces recorded under dynamic N_2 atmosphere. However, the oxidation of Fe(II) by CO_2 at the endothermal peak temperature takes place simultaneously (*17*).

Due to the complexity of this thermal behavior, various phases could be identified as intermediates. Table I summarizes the products of thermal decomposition of the mixed carbonates after 1 hr of isothermal treatment in air at different temperatures. These results evidence the complexity of this system, which is due to the multiple oxidation states and structural possibilities of Mn in oxide compounds that are affected by the nonequilibrium conditions of this preparative route. From these results, it is shown that monophasic spinel products can be obtained only at 400°C under these experimental conditions (Fig. 2). In order to obtain higher temperature monophasic spinels, the thermal decomposition of the Mn/Fe carbonates was carried out by different procedures. In this way, it was found that the occurrence of α-sesquioxide phases at 600°C could be avoided by removing gases generated in the decomposition by passing an inert gas over the sample. The XRD patterns of these samples are shown in Fig. 2.

The chemical composition and crystallographic data of the products obtained at 400 and 600°C are collected in Table II. The average oxidation states of metal ions in both sets of samples are higher than that corresponding to an M_3O_4 stiochiometry. At 400°C, the O/*M* (*M* = total metal content)

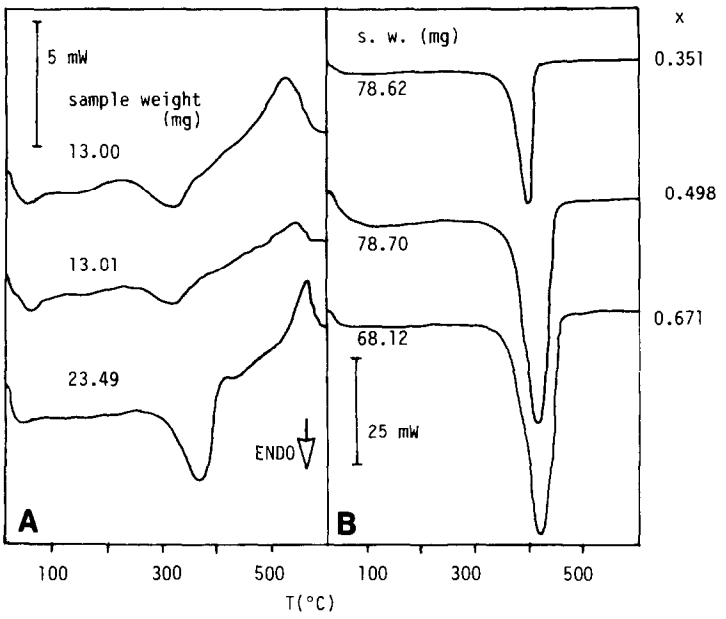

FIG. 1. DSC traces of Mn/Fe carbonates recorded under static air atmosphere.

TABLE I

DECOMPOSITION PRODUCTS OF Mn/Fe CARBONATES IN THE THERMAL TREATMENT UNDER STATIC AIR ATMOSPHERE AT DIFFERENT TEMPERATURES

			x		
T (°C)	0.000	0.351	0.498	0.671	1.000
400	γ	γ	γ	γt	γt
500	α	γ	γ + (α)	γ + c	γt + c
600	α	γ + (α)	γ + (c)	γ + c	c + γt
700	α	α + γ	c + γ	c + (γ)	c + (γt)
900	α	α + (γ)	c + (γ)	c + (α)	c
1100	α	γ	γ	γ	γt

x = Mn/(Mn + Fe). α, corundum structure; γ, spinel structure; c, C-type oxide structure; γt, Mn_3O_4 (tetragonal spinel) structure.

ratios are in the 1.5–1.6 range. The presence of high oxidation states in Mn-containing spinels has also been reported in other carbonate decomposition products (*10, 18, 19*). This implies the presence of cation vacancies in the spinel structure that were ordered in a γ-Fe_2O_3-type superstructure for $x < 0.640$ as shown by XRD (Fig. 2). The fact that high Mn contents condition the absence of superstructure lines in the XRD pattern may be connected with divergences in crystallinity of the solids or changes in the vacancy distribution in octahedral/tetrahedral sites, as discussed below. On the other hand, the superstructure lines are more intense for the samples obtained at low temperature. This fact is in agreement with a high vacancy content, especially in octahedral sites, which is also derived from the chemical and Mössbauer data, as shown below.

On the other hand, the spinel oxide phases found at both temperatures were cubic except for high Mn contents ($x > 0.64$) that condition the occurrence of tetragonal distortions due to the Jahn–Teller effect. The effect occurs for Mn contents higher than those found in the Co–Mn–O system (*10, 20*), indicating a lower Mn(III) content, especially in octahedral oxygen coordination.

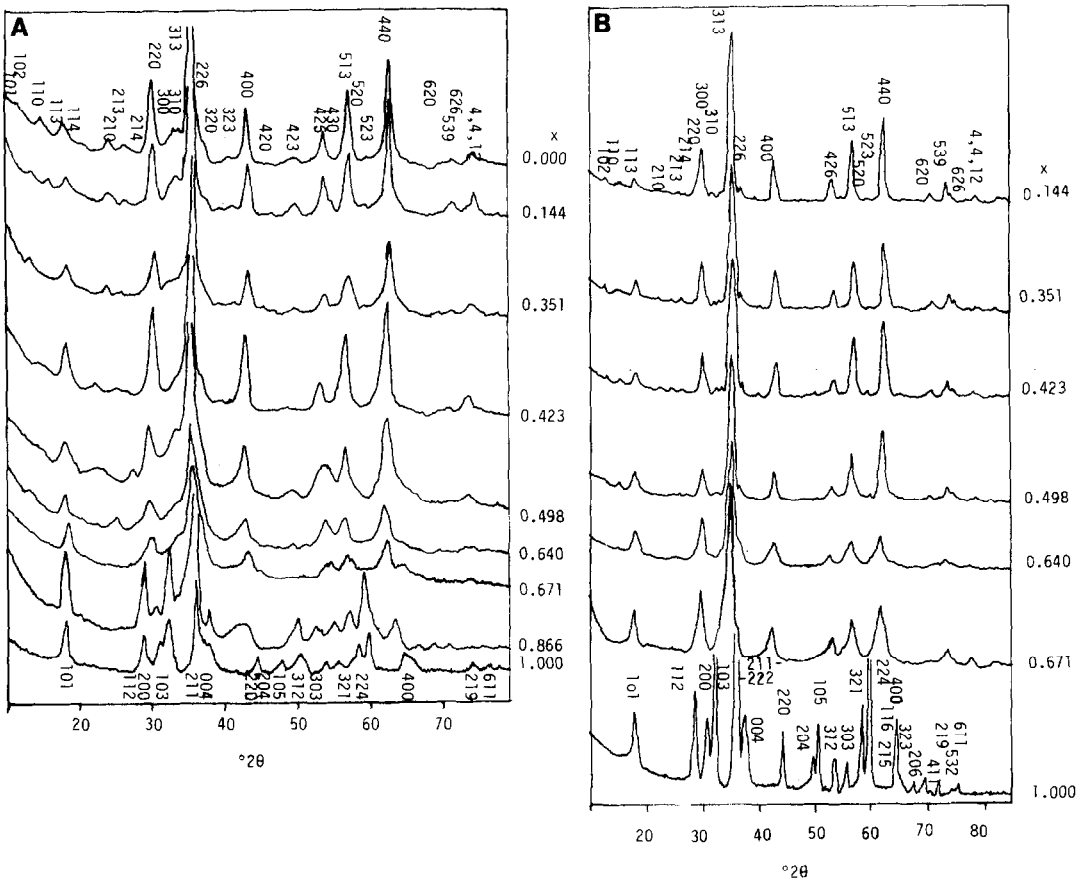

FIG. 2. XRD plots of Mn/Fe spinel oxides of general formula $Fe_{3-x}Mn_xO_{4+y}$ obtained by thermal decomposition of the precursor carbonates at 400 (A) and 600°C (B).

For cubic spinels, the unit cell parameters at both preparation temperatures are included in Table II. This parameter increases with Mn content, probably due to the higher ionic radius of Mn(II) and Mn(III) as compared with Fe(III). However, at 400°C the increase in a is less marked, probably indicating the higher presence of other smaller ions as Mn(IV). The a value observed for $x = 0.35$ is lower than that reported for $MnFe_2O_4$ (*21*) and this fact is in correspondence with the high cation-vacancy content in our samples and the higher oxidation state of metal ions.

Table III shows the values of BET surface area and the results of line-broadening analysis. At 400°C, a high dispersion of the samples is evidenced by the low values of crystallite size and moderately high values of specific surface area. It is commonly found that the preparation of spinel oxides by the low temperature decomposition of suitable precursor compounds leads to fine and ultrafine particles (*22, 23*). The electron micrographs in Fig. 3 are in agreement with these observations. It should be noted that the samples are formed by aggregates of primary particles, thus leading to BET surface values lower than those corresponding to the observed crystallite sizes. On the other

TABLE II

CHEMICAL COMPOSITION AND STRUCTURAL DATA OF MIXED Mn/Fe SPINEL OXIDES

T (°C)	400			600		
x	O/M[a]	a[b]	c[b]	O/M	a	c
0.000	1.500	8.343		1.500		c
0.144	1.569	8.365		1.489		8.419
0.351	1.607	8.378		1.456		8.435
0.423	1.600	8.397		1.477		8.468
0.498	1.593	8.432		1.467		8.472
0.640	1.599	8.442[d]		1.434		8.530
0.671	1.609	8.448[d]		1.441		8.599[d]
0.866	1.600	5.855	9.497	1.387	5.843	9.485
1.000	1.582	5.825	9.554	1.336	5.762	9.470

[a] ±0.003.
[b] ±0.002 Å.
[c] α-Fe_2O_3.
[d] Pseudocubic phases.

TABLE III

BET SURFACE, CRYSTALLITE SIZE AND MICROSTRAINS OF MIXED Mn/Fe SPINEL OXIDES

x	$S_{BET}(m^2g^{-1})$	D_{400}(Å)	$\hat{e}_{400} \times 10^{-3}$	D_{440}(Å)	$\hat{e}_{440} \times 10^{-3}$	I_{220}/I_{400}
			400°C			
0.144	52.7	215	2.4	167	0	1.22
0.351	71.1	126	5.3	131	0	1.16
0.423	60.1	143	3.7	103	1.7	1.10
0.498	64.4	135	3.9	95	3.1	0.87
0.640	89.8	81	6.3	116	4.2	0.80[a]
0.671	40.1	61	6.9	136	7.9	0.66[a]
			600°C			
0.144	4.8	[b]	5.5	[b]	1.9	1.73
0.351	10.4	[b]	5.5	[b]	3.1	1.23
0.423	22.2	3000	3.4	3000	3.4	1.10
0.498	23.7	281	3.4	271	2.1	1.16
0.640	21.2	90	6.5	147	9.0	1.02
0.671	12.2	98	7.8	108	9.4	1.54[a]

[a] Pseudocubic phases.
[b] Values higher than the limits of determination of the method.

hand, there is not a clear tendency of these parameters with x. At 600°C, the degree of sample dispersion is lower.

For a sample with $x = 0.144$, Fig. 3 shows particle sizes ranging from 500 to 3000 Å. The primary particles show preferred $\langle 1\bar{1}0 \rangle$ zones, an orientation which is commonly found in acicular (ex-α-FeOOH) (*24*) or layered (ex-$FeOOH_3$) (*25*) γ-Fe_2O_3. For a sample with $x = 0.498$, the $\langle 001 \rangle$ zone axis elec-

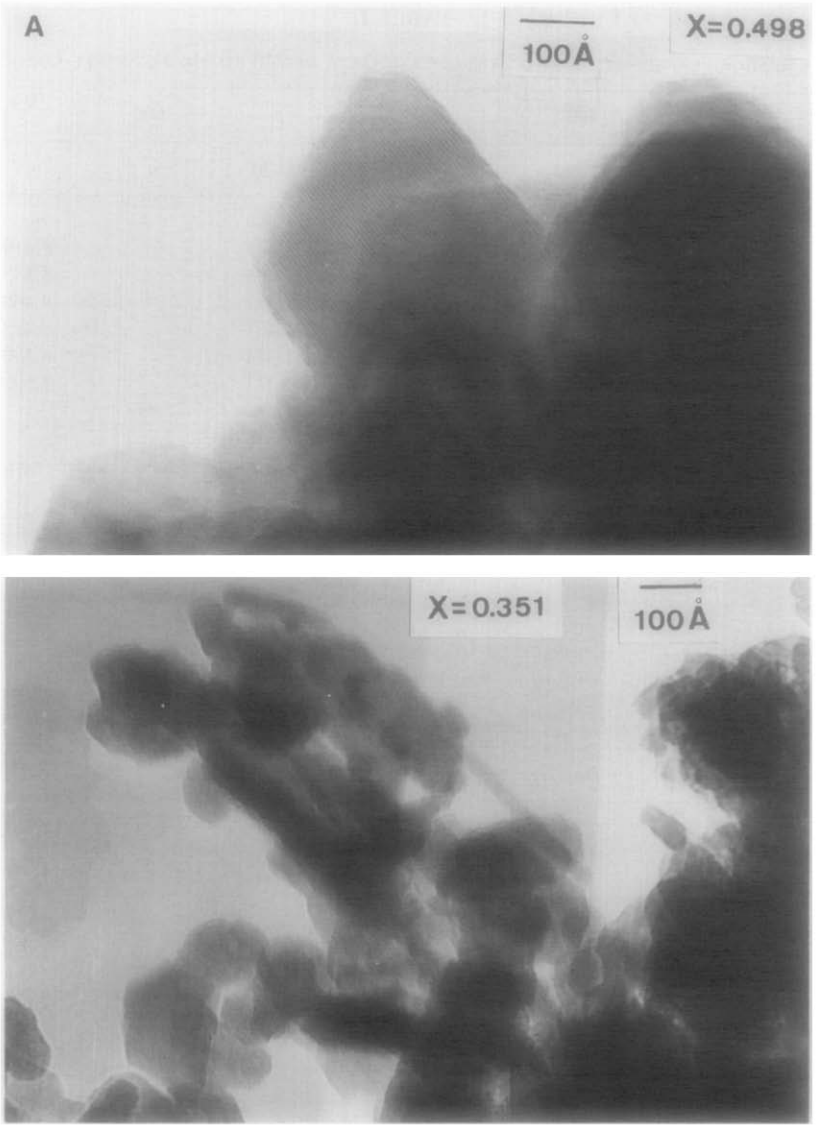

FIG. 3. (A) Electron micrographs of Fe/Mn spinel oxides $Fe_{3-x}Mn_xO_{4+y}$ obtained at 400°C. (B) Samples obtained at 600°C showing ⟨001⟩ and ⟨1$\bar{1}$0⟩ orientations. The drawing of the electron diffraction pattern with ⟨001⟩ orientation shows smaller spots corresponding to a *P* cubic lattice.

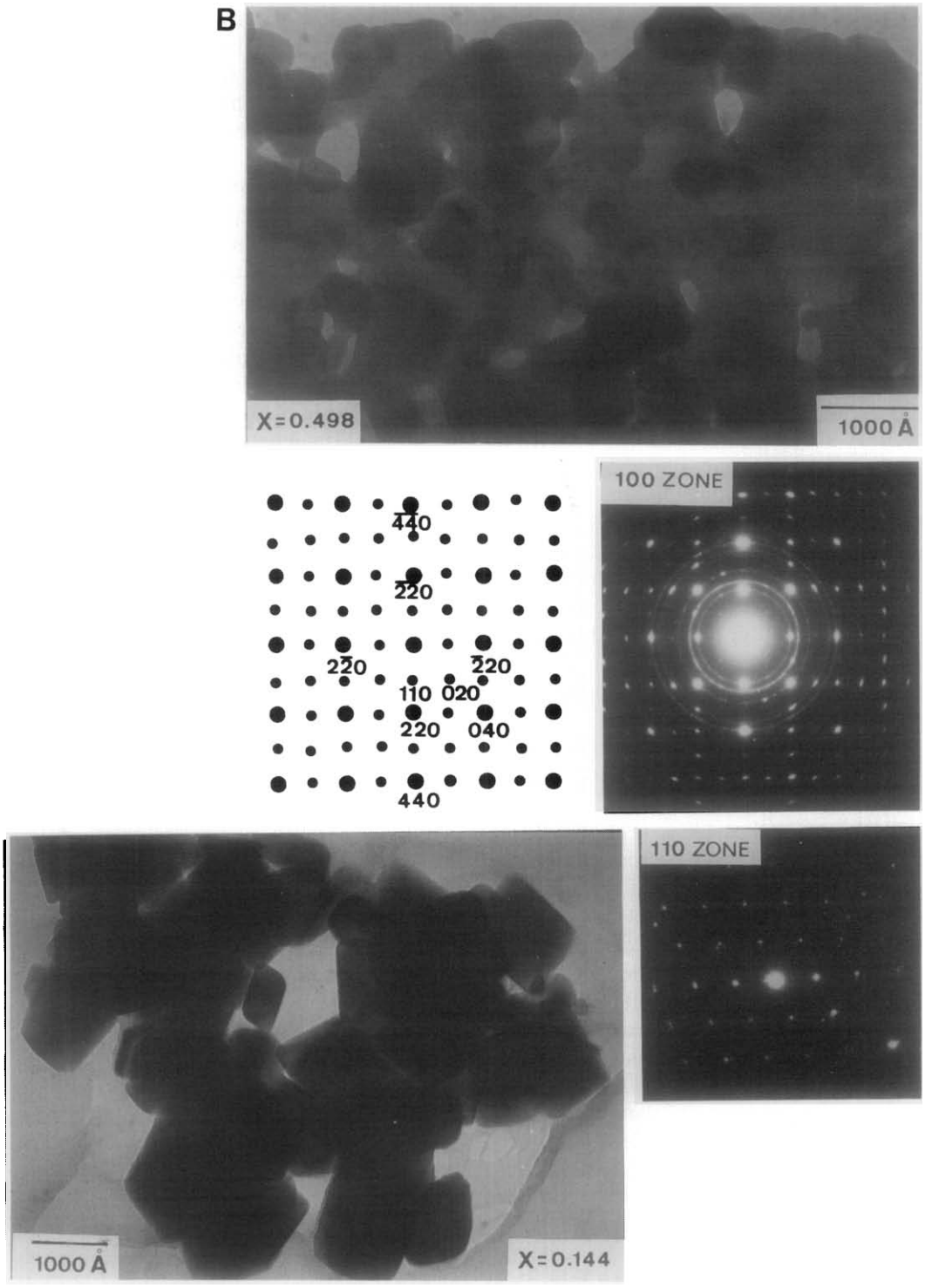

FIG. 3.—*Continued*

tron diffraction pattern shows (110) and (020) weak spots, corresponding to a P cubic lattice. Boudeulle *et al.* (*26*) showed that a statistical distribution of vacancies could occur by reducing the F cubic symmetry of the spinel to a P lattice. However, one of the resulting space groups, $P4_332$, does not allow (020) spots. From these results and XRD data, the presence of a primitive tetragonal superlattice with $c \simeq 3a$ cannot be discarded. It should be noted that the presence of vacancy ordering in superstructure was pointed out by Gillot *et al.* (*8*) from IR data for compositions with $x < 0.5$.

Although the preparation at higher temperature generally increases the size of the coherently diffracting domains, a higher content of microstrains is simultaneously observed in these samples. This fact may probably be in connection with the proximity of the preparation temperature to the $\gamma \rightarrow \alpha$ phase transition, thus being highly distorted metastable phases. In addition, the sintering phenomena may lead to distorted regions in the bulk of the material in spinel oxides (*27*).

As a complementary technique in the analysis of vacancy distribution, Fig. 4 shows the RT Mössbauer spectra of the samples prepared at 400°C. These patterns shows a central doublet component that increases its intensity with Mn content relative to the hyperfine sextet component. Such a doublet component cannot be ascribed to the presence of undecomposed carbonate as the chemical shift of this phase is higher (*28*); besides, no lines of carbonate are present in XRD patterns. The occurrence of this doublet can be explained by assuming the presence of a variable fraction of superparamagnetic particles with sizes sufficiently small to produce a fast relaxation of the magnetic moment (*29*). Alternatively, the presence of isolated ferrimagnetic regions surrounded by non magnetic structural components may also lead to a similar effect in the Mössbauer spectra. This explanation was used in the study of Mn–Zn (*2*) and Ni–Zn (*30*) spinel ferrites. In our case there are no diamagnetic ions as Zn^{+2}, but this role could be played as well by the cation vacancies.

The changes in BET surface and crystallite size cannot explain satisfactorily the increase in the intensity of the doublet signal with Mn content, although their contribution to the occurrence of the doublet cannot be discarded. On the other hand, it should be noted that the isolation of Fe(III) from magnetic interactions can originate a collapse in the hyperfine splitting. The main cause for the magnetic cooperative behavior of the spinels is known to be the antiferromagetic A–B superexchange interactions (*4*). Thus, the A–A and B–B interactions have little effect on the Mössbauer spectra (*31*). As the quadrupole splitting is only observed for octahedrally coordinated ions, a significant amount of vacancies should lie on tetrahedral positions to produce the isolating effect on the B sites.

The presence of vacancies in octahedral positions leads to the above-mentioned γ-Fe_2O_3 superstructure lines in the XRD patterns for Mn contents lower than $x = 0.640$. This fact is in correspondence with the XRD intensity ratio I_{220}/I_{400} (Table III). This ratio decreases with Mn content, and is indicative of a progressive displacement of the vacancies from octahedral to tetrahedral positions, in contrast to previously described data for $MnFe_2O_{4+\delta}$ ($\delta \geq 0$) (*6*). On the other hand, the increase in the number of vacancies in tetrahedral positions with Mn content agrees with the interpretation of the enhancement of the intensity of the doublet component in the Mössbauer spectra based on isolating effects. However, the difficulty of separation of isolating effects from surface effects that are commonly found in these highly dispersed materials cannot be avoided, as evidenced in the study of ^{57}Fe-

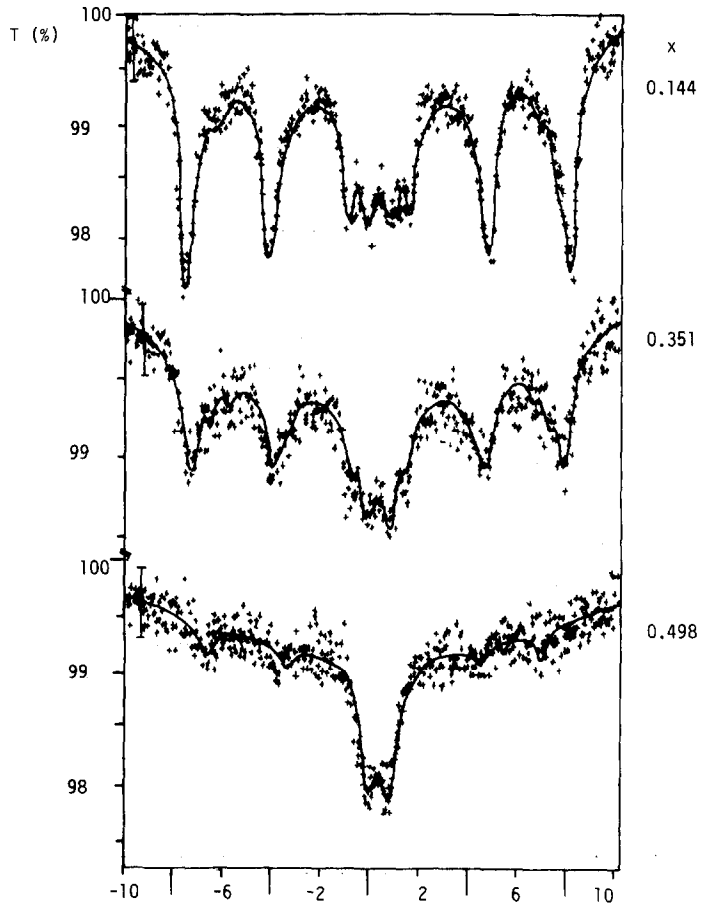

FIG. 4. Mössbauer spectra of three selected samples of Mn/Fe spinel oxides obtained at 400°C. Vertical bars indicate the standard deviation of each measurement.

enriched samples of micronized γ-Fe_2O_3 (*32*).

The RT Mössbauer spectra of the spinel samples prepared at 600°C are included in Fig. 5. The most relevant aspect of these spectra is the absence of quadrupole splitting signals. This is an expected result, as crystallite size is higher and BET surface is lower at this temperature (Table III), simultaneous to a decrease in oxidation state, which leads to a lower vacancy content. For these samples, the unit cell parameters pointed to a higher Mn(III)/Mn(IV) ratio and the observed y values of $Fe_{1-x}Mn_xO_{4+y}$ are lower than those found at 400°C.

Conclusions

The thermal behavior of Fe/Mn mixed carbonates is complex, and several phases can be identified as the products of the thermal decomposition at different temperatures.

The thermal decomposition of Fe/Mn mixed carbonates at low temperature (400°C) leads to spinel phases with a high

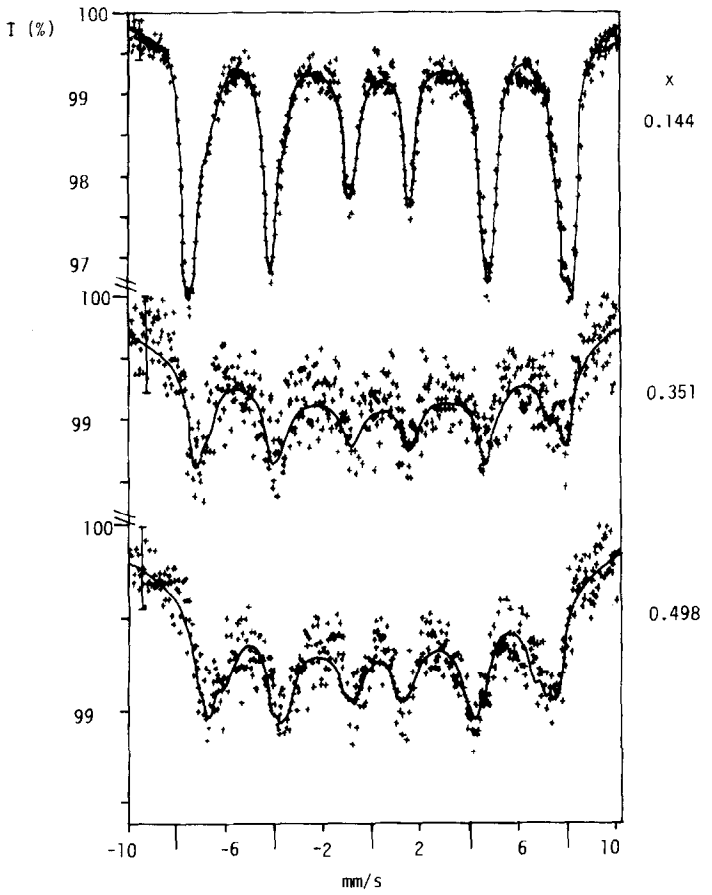

FIG. 5. Mössbauer spectra of three selected samples of Fe/Mn spinel oxides obtained at 600°C. Vertical bars indicate SD.

vacancy content, whereas lower oxidation states are achieved when the decomposition is carried out under less oxidizing conditions at high temperature (600°C).

The vacancies are placed preferentially in octahedral positions, and they are ordered in a γ-Fe_2O_3-type superstructure at both temperatures. However, when the vacancy content is high (400°C samples), some of them are displaced to tetrahedral positions.

The vacancies in tetrahedral positions may produce an intense decrease in the hyperfine interactions, which, together with the particle size effects, originates the occurrence of a quadrupole doublet in the Mössbauer spectra of 400°C samples.

Acknowledgments

The authors acknowledge CICYT and PFPI for financial support.

References

1. K. NAITO, H. INABA, AND H. YAGI, *J. Solid State Chem.* **36,** 28 (1981).
2. M. PETRERA, A. GENNARO, AND N. BURRIESCI, *J. Mater. Sci.* **17,** 429 (1982).
3. T. TSUJI, Y. ASAKURA, T. YAMASHITA, AND K. NAITO, *J. Solid State Chem.* **50,** 273 (1983).

4. G. A. SAWATZKY, F. VEN DER WOUDE, AND A. H. MORRISH, *Phys. Rev* **187,** 747 (1969).
5. M. TANAKA, T. MIZOGUCHI, AND Y. AIYAMA, *J. Phys. Soc. Japan* **18,** 1091 (1963).
6. G. D. RIECK AND F. C. M. DRIESSENS, *Acta Crystallogr.* **20,** 521 (1966).
7. B. GILLOT AND M. EL GUENDOUZI, *React. Solids* **1,** 139 (1986).
8. B. GILLOT, M. EL GUENDOUZI, AND A. ROUSSET, *J. Solid State Chem.* **68,** 285 (1987).
9. B. GILLOT, M. EL GUENDOUZI, M. LAARG, P. TAILHADES, AND A. ROUSSET, *J. Mater. Sci.* **23,** 3342 (1988).
10. J. M. JIMENEZ MATEOS, J. MORALES, AND J. L. TIRADO, *J. Solid State Chem.* **82,** 87 (1989).
11. J. M. JIMENEZ MATEOS, J. MORALES, AND J. L. TIRADO, *React Solids* **7,** 235 (1989).
12. K. VIDYASAGAR, J. GOPALAKRISHNAN, AND C. N. R. RAO, *Inorg. Chem.* **23,** 1206 (1984).
13. TH. H. DE KEIJSER, E. MITTENMEIJER, AND H. C. R. ROZENDAAL, *J. Appl. Crystallog.* **16,** 309 (1983).
14. S. BRUNAUER, P. H. EMMETT, AND E. TELLER, *J. Amer. Ceram. Soc.* **60,** 309 (1938).
15. C. N. R. RAO AND J. GOPALAKRISHNAN, *Acc. Chem. Res.* **20,** 228 (1987).
16. R. C. MACKENZIE, "Differential Thermal Analysis," Academic Press, London (1982).
17. P. K. GALLAGHER, *Mater. Res. Bull.* **16,** 141 (1981).
18. A. FELTZ, W. LUDWIG, AND CH. FELBEL, *Z. Anorg. Allg. Chem.* **540/541,** 36 (1986).
19. A. FELTZ AND J. JÄGER, *React. Solids* **6,** 119 (1988).
20. S. NAKA, M. INAGAKI, AND T. TANAKA, *J. Mater Sci.* **7,** 441 (1972).
21. JCPDS, Power Diffraction File 10-319 (1959).
22. P. RAVINDRANATHAN, G. V. MAHESH, AND K. C. PATIL, *J. Solid State Chem.* **66,** 20 (1987).
23. P. PESHEV, A. TOSHEV, AND G. GYUROX, *Mater. Res. Bull.* **24,** 33 (1989).
24. A. E. BERKOWITZ, R. P. GOEHNER, E. L. HALL, AND P. J. FLANDERS, *J. Appl. Phys.* **57,** 3928 (1985).
25. J. MORALES, J. L. TIRADO, AND C. VALERA, *J. Amer. Ceram. Soc.* **72,** 1244 (1989).
26. M. BOUDEULLE, H. BATIS-LANDOULSI, CH. LECLERCQ, AND P. VERGNON, *J. Solid State Chem.* **48,** 21 (1983).
27. L. HERNAN, J. MORALES AND J. L. TIRADO, *J. Colloid Interface Sci.* **110,** 172 (1986).
28. P. K. GALLAGHER, K. W. WEST, AND S. ST. J. WARNE, *Thermochim Acta* **50,** 41 (1982).
29. A. M. VAN DER KRAAN, *J. Phys. (Paris)* **32,** C1-1034 (1971).
30. Y. ISHIKAWA, *J. Appl. Phys.* **35,** 1054 (1964).
31. N. N. GREENWOOD AND T. C. GIBB, *"Mössbauer Spectroscopy,"* Chapman and Hall, London (1971).
32. A. H. MORRISH, K. HANEDA, AND P. J. SCHURER, *J. Phys. (Paris)* **37,** C6-301 (1976).